

# Large voltage-tunable spin valve based on a double quantum dot

Patrycja Tulewicz,<sup>1,\*</sup> Kacper Wrześniewski,<sup>1</sup> Szabolcs Csonka,<sup>2</sup> and Ireneusz Weymann<sup>1,†</sup>

<sup>1</sup>*Institute of Spintronics and Quantum Information,  
Faculty of Physics, Adam Mickiewicz University,  
ul. Uniwersytetu Poznańskiego 2, 61-614 Poznań, Poland*

<sup>2</sup>*Department of Physics, Budapest University of Technology and Economics and MTA-BME  
"Momentum" Nanoelectronics Research Group, H-1111 Budapest, Budafoki út 8., Hungary*

(Dated: March 31, 2021)

We study the spin-dependent transport properties of a spin valve based on a double quantum dot. Each quantum dot is assumed to be strongly coupled to its own ferromagnetic lead, while the coupling between the dots is relatively weak. The current flowing through the system is determined within the perturbation theory in the hopping between the dots, whereas the spectrum of a quantum dot-ferromagnetic lead subsystem is determined by means of the numerical renormalization group method. The spin-dependent charge fluctuations between ferromagnets and quantum dots generate an effective exchange field, which splits the double dot levels. Such field can be controlled, separately for each quantum dot, by the gate voltages or by changing the magnetic configuration of external leads. We demonstrate that the considered double quantum dot spin valve setup exhibits enhanced magnetoresistive properties, including both normal and inverse tunnel magnetoresistance. We also show that this system allows for the generation of highly spin-polarized currents, which can be controlled by purely electrical means. The considered double quantum dot with ferromagnetic contacts can thus serve as an efficient voltage-tunable spin valve characterized by high output parameters.

## I. INTRODUCTION

Quantum dot spin valves can be regarded as basic building blocks of quantum spintronics and nanoelectronics [1, 2]. Such devices typically consist of a nanoscale object, a quantum dot or a molecule, attached by tunnel barriers to external ferromagnetic contacts [3–7]. The current flowing through these systems strongly depends on the mutual orientation of the magnetic moments of ferromagnetic leads and can be additionally controlled by a gate voltage. In conventional spin valves, the tunneling current is larger when the configuration of the leads' magnetizations is parallel as compared to the case when the magnetic moments of the leads form an antiparallel configuration [8]. This is associated with the asymmetry between the spin-dependent tunneling processes in these two configurations [9, 10]. The situation becomes more interesting when strong electron correlations are present in the system, such as the ones driving the Kondo effect [11–13]. Then, an inverse tunnel magnetoresistance effect may develop in the system [5, 14, 15]. Moreover, the current flowing through the device can become highly spin-polarized [16, 17]. In fact, a single quantum dot based spin polarizer, with nearly perfect electrically-controlled spin polarization of the tunneling current, has been recently proposed [18]. The operation of such device is based on the exchange field that is induced when quantum dot or molecule becomes strongly coupled to ferromagnetic reservoirs [19–21]. By spin-dependent charge fluctuations, the orbital level of the dot becomes spin-

split and consequently mainly the electrons with favorable spin orientation are transferred through the system. Moreover, it turns out that the exchange field results in high spin polarization of the local density of states, which is responsible for controllable spin rectification of the current [18]

From a theoretical point of view, the transport properties of quantum dot spin valves, consisting of single dots coupled to ferromagnetic leads, have already been a subject of extensive studies, both in the weak [3, 4, 8, 22–24] and in the strong coupling regime [15, 19–21, 25]. Moreover, more complex structures involving double quantum dots with ferromagnetic leads have also been explored [26–29]. As far as the experimental progress is concerned, most experiments on nanoscopic spin valves have been devoted to transport properties of single dot or molecular structures [5–7, 14, 17, 30–34], whereas double quantum dot spin valves have been implemented only very recently [35].

In this paper we develop the theory of transport through a double quantum dot strongly coupled to external ferromagnetic leads, while the coupling between the two dots is assumed to be relatively weak, see Fig. 1(a). In such geometry, the spin-resolved transport strongly depends on the magnitude and sign of the exchange field present on each quantum dot. In fact, such field plays a role of a local magnetic field that can be controlled by the gate voltage applied to the dot. The possibility of splitting the level of a given dot at will provides the opportunity for implementing a spin valve with magnetoresistive response much exceeding that obtained for external-magnetic-field controlled behavior [35]. We show that the particular geometry of the system considered in this work allows us for obtaining enhanced spin valve behav-

\* pattul@st.amu.edu.pl

† weymann@amu.edu.pl

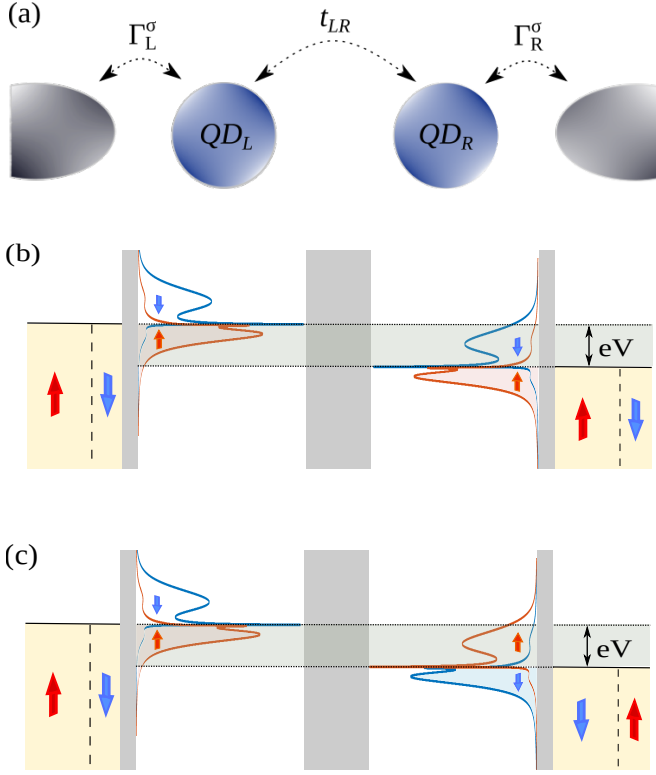


FIG. 1. (a) Schematic of the considered system. It consists of two quantum dots: the left ( $\alpha = L$ ) and right ( $\alpha = R$ ) one, attached to the corresponding metallic ferromagnetic leads with the spin-dependent coupling strengths  $\Gamma_\alpha^\sigma$ . The coupling between the dots is represented by the hopping matrix element  $t_{LR}$ . The diagrams for the parallel and antiparallel configuration of leads' magnetic moments, demonstrating the spin valve behavior, are presented in (b) and (c), respectively. The quantum dots are assumed to be occupied by a single electron, such that the density of states is characterized by large spin asymmetry due to the exchange field. The magnitude and spin polarization of the current flowing through the system is determined by the polarization of the local density of states in the bias window  $eV$ . Due to the mismatch of densities of states, the current in the parallel configuration is much smaller compared to the current flowing in the antiparallel configuration, which is additionally highly spin polarized.

ior, ensuring full control of spin-dependent transport by the bias and gate voltages. In particular, in the linear response regime, we demonstrate that one can obtain a considerable, both positive and inverse, tunnel magnetoresistance. On the other hand, in the nonlinear response regime, we predict a perfect spin polarization of the flowing current and a greatly enhanced magnetoresistance when the sign of the exchange field is different in each dot, which can be obtained by appropriate tuning of gate voltages. Our work reveals thus that double quantum dots strongly attached to external ferromagnetic leads can be regarded as fully voltage-controllable spin valves with very prospective spin-resolved properties.

This paper is structured as follows. Section II is devoted to theoretical description, where the model, method and formulas for transport quantities are presented. In Sec. III we discuss the possibility of gate-voltage control of double-dot spin valve in the linear response regime, whereas Sec. IV is devoted to the spin-resolved transport properties when a finite bias voltage is applied to the system. Finally, the paper is concluded in Sec. V.

## II. THEORETICAL DESCRIPTION

The schematic of the considered double quantum dot spin valve is presented in Fig. 1(a). The system consists of two single-level quantum dots strongly attached to external ferromagnetic leads with coupling strengths  $\Gamma_\alpha^\sigma$ , where  $\alpha = L$  ( $\alpha = R$ ) for the left (right) lead, and weakly connected to each other through the hopping matrix elements  $t_{LR}$ . The ferromagnetic leads are assumed to form either parallel or antiparallel magnetic configuration. The total Hamiltonian of the system can be written as

$$H = H_{0L} + H_{0R} + H_{TL} + H_{TR} + H_{DQL} + H_{DQR} + H_T, \quad (1)$$

where  $H_{0\alpha}$  models the noninteracting electrons in the left ( $\alpha = L$ ) and right ( $\alpha = R$ ) ferromagnetic electrode,

$$H_{0\alpha} = \sum_{k\sigma} \varepsilon_{\alpha k\sigma} c_{\alpha k\sigma}^\dagger c_{\alpha k\sigma}, \quad (2)$$

where the operator  $c_{\alpha k\sigma}^\dagger$  creates an electron with momentum  $k$  spin  $\sigma$  of energy  $\varepsilon_{\alpha k\sigma}$  in the lead  $\alpha$ . The tunneling between the corresponding quantum dot and electrode  $\alpha$  is modeled by

$$H_{T\alpha} = \sum_{k\sigma} t_\alpha^\sigma (c_{\alpha k\sigma}^\dagger d_{\alpha\sigma} + d_{\alpha\sigma}^\dagger c_{\alpha k\sigma}), \quad (3)$$

with  $d_{\alpha\sigma}^\dagger$  ( $d_{\alpha\sigma}$ ) being the creation (annihilation) operator of a spin- $\sigma$  electron in the quantum dot  $\alpha$  and  $t_\alpha^\sigma$  denoting the tunnel matrix elements, assumed to be momentum independent. The strength of the tunnel coupling between the corresponding quantum dot and electrode can be written as  $\Gamma_\alpha^\sigma = \pi \rho_\alpha^\sigma |t_\alpha^\sigma|^2$ , where  $\rho_\alpha^\sigma$  is the spin-dependent density of states of lead  $\alpha$ . The coupling constants can be more conveniently written in terms of spin polarization of lead  $\alpha$ ,  $p_\alpha = (\Gamma_\alpha^\uparrow - \Gamma_\alpha^\downarrow) / (\Gamma_\alpha^\uparrow + \Gamma_\alpha^\downarrow)$ , as  $\Gamma_\alpha^\sigma = (1 + \hat{\sigma} p_\alpha) \Gamma_\alpha$ , where  $\hat{\sigma} = +(-)$  for majority (minority) spin band and  $\Gamma_\alpha = (\Gamma_\alpha^\uparrow + \Gamma_\alpha^\downarrow) / 2$ . The hopping between the two quantum dots is described by

$$H_T = \sum_{\sigma} t_{LR} (d_{L\sigma}^\dagger d_{R\sigma} + d_{R\sigma}^\dagger d_{L\sigma}). \quad (4)$$

Finally, the Hamiltonian for quantum dot  $\alpha$  is given by

$$H_{DQ\alpha} = \sum_{\sigma} \varepsilon_{\alpha} n_{\alpha\sigma} + U_{\alpha} n_{\alpha\uparrow} n_{\alpha\downarrow}, \quad (5)$$

where  $n_\alpha = n_{\alpha\uparrow} + n_{\alpha\downarrow}$  with  $n_{\alpha\sigma} = d_{\alpha\sigma}^\dagger d_{\alpha\sigma}$ . The Coulomb correlations on each quantum dot are denoted by  $U_\alpha$ . In our considerations, it is assumed that the coupling between the two dots is much weaker than the coupling of each dot to its contact. Moreover, we also assume that the on-site Coulomb correlations are much larger than the correlations between the two dots and therefore the latter ones can be neglected.

To determine the current flowing through the system, we perform a perturbative expansion in  $H_T$ . Consequently, we rewrite the Hamiltonian (1) as,  $H = H_L + H_R + H_T$ , where  $H_\alpha$  models the dot  $\alpha$  coupled to the corresponding lead. It is given by the Anderson Hamiltonian [36],  $H_\alpha = H_{0\alpha} + H_{T\alpha} + H_{QD\alpha}$ . Then, in the lowest-order with respect to hopping matrix elements  $t_{LR}$ , we can express the current flowing in the spin channel  $\sigma$  as [18, 37]

$$I_\sigma(V) = \frac{1}{eR_\sigma} \int_{-\infty}^{\infty} d\omega \mathcal{A}_L^\sigma(\omega) \mathcal{A}_R^\sigma(\omega - eV) \times [f(\omega) - f(\omega - eV)], \quad (6)$$

where  $f(\omega)$  is the Fermi-Dirac distribution function and the resistance of the junction between the two quantum dots is given by,  $R_\sigma = \hbar / (2\pi e^2 A_{L0}^\sigma A_{R0}^\sigma t_{LR}^2)$ , with  $A_{\alpha 0}^\sigma = 1/\pi \Gamma_\alpha^\sigma$ .  $\mathcal{A}_\alpha^\sigma(\omega)$  is the normalized spin-dependent spectral function (local density of states) of the quantum dot  $\alpha$  coupled to the corresponding lead, as described by  $H_\alpha$ . Note that we assume the left lead to be grounded, while the voltage is applied to the right lead, see Fig. 1. In the following, we assume that the quantum dots have comparable charging energies and are coupled with the same strength to the leads, i.e.  $U_L = U_R \equiv U$  and  $\Gamma_L = \Gamma_R \equiv \Gamma$ . We also set  $t_{LR} = \Gamma/10$ . Moreover, we assume that the electrodes are made of the same material, such that  $p_L = p_R = p$ . Taking into account realistic quantum dot parameters,  $\Gamma \approx 1\text{meV}$  and  $t_{LR} \approx 0.1\text{meV}$ , one finds  $R_\sigma \sim \text{M}\Omega$ , which yields the maximum current on the order of tens of nA.

In this work we are interested in the spin-dependent transport properties of the system at low temperatures both in the linear and nonlinear response regimes. The main computational task is to determine the spin-resolved spectral function  $A_\alpha^\sigma(\omega)$  of the quantum dot-ferromagnetic lead subsystem modeled by  $H_\alpha$ . The spectral function is given by,  $A_\alpha^\sigma(\omega) = -\text{Im}[G_\alpha^\sigma(\omega)]/\pi$ , where  $G_\alpha^\sigma(\omega)$  is the Fourier transform of the retarded Green's function of the corresponding quantum dot level,  $G_\alpha^\sigma(t) = -i\Theta(t)\langle\{d_{\alpha\sigma}^\dagger(0), d_{\alpha\sigma}(t)\}\rangle$ . Because each dot is strongly coupled to its own lead, while the hopping between the two dots is assumed to be the smallest energy scale, we can use the numerical renormalization group (NRG) method [38–40] to find  $A_\alpha^\sigma(\omega)$  separately for each quantum dot. This method allows us to accurately account for all the correlation effects between the quantum dot and ferromagnet. In calculations, we use the discretization parameter  $\Lambda = 2$  and keep at least  $N_K = 1024$  low-energy states in the numerical procedure. Moreover, to increase the accuracy of spectral functions, we employ

the  $z$ -averaging trick [41] and make use of the optimal broadening method [42].

For nonmagnetic leads, at sufficiently low temperatures, the quantum dot-electrode subsystem exhibits the Kondo effect [11, 13]. On the other hand, for ferromagnetic leads, the spin-resolved charge fluctuations between the dot and ferromagnet give rise to an effective exchange field  $\Delta\varepsilon_{\text{exch}}$  [19]. Such field can spin-split the quantum dot level and, consequently, suppress the Kondo effect if the splitting becomes larger than the corresponding Kondo temperature [31–33]. Consequently, the exchange field plays a role of a highly-tunable local magnetic field acting on a given dot. Analytically, this field can be estimated within the second-order perturbation theory, and at zero temperature, for quantum dot  $\alpha$ , it is given by [19, 21]

$$\Delta\varepsilon_{\text{exch}}^\alpha = \frac{2\Gamma p}{\pi} \ln \left| \frac{\varepsilon_\alpha}{\varepsilon_\alpha + U} \right|. \quad (7)$$

It is evident that the field changes sign when the dot level crosses the particle-hole symmetry point,  $\varepsilon_\alpha = -U/2$ . Moreover, the exchange field is responsible for high spin polarization of the spectral functions [18]. This can be seen in Figs. 1(b) and (c), which demonstrate the principle of operation of the considered double quantum dot spin valve in the nonequilibrium regime. The presented spectral functions were calculated by NRG for  $\varepsilon_L = \varepsilon_R = -0.3U$ , i.e. when  $\Delta\varepsilon_{\text{exch}}^\alpha$  is finite for each dot, and clearly reveal a strong spin asymmetry. Note also the presence of a small resonance due to the Kondo effect, which is pinned to the lead's chemical potential. The large spin valve behavior can be obtained either by tuning the positions of the quantum dot levels, which can be done with appropriate gate voltages or by changing the magnetic configuration of the device. The latter mechanism is sketched in Figs. 1(b) and (c).

### III. LINEAR RESPONSE REGIME

In this section we discuss the linear-response behavior of the system. The linear conductance in the spin channel  $\sigma$  can be found from

$$G_\sigma = \frac{1}{R_\sigma} \int_{-\infty}^{\infty} d\omega \mathcal{A}_L^\sigma(\omega) \mathcal{A}_R^\sigma(\omega) \left( -\frac{\partial f(\omega)}{\partial \omega} \right). \quad (8)$$

As results from the above formula, for low temperatures the linear conductance is proportional to the product of the two spectral functions at the Fermi level. Thus, appropriate tuning of the quantum dot levels, which can be experimentally achieved by gate voltages, can greatly affect the conductance of the system. Moreover, it will determine the spin-resolved properties of the considered spin valve, allowing for an accurate tuning of both the tunnel magnetoresistance and the spin polarization of the current in a fully electrical manner, without the need for applying external magnetic field. Nevertheless, besides

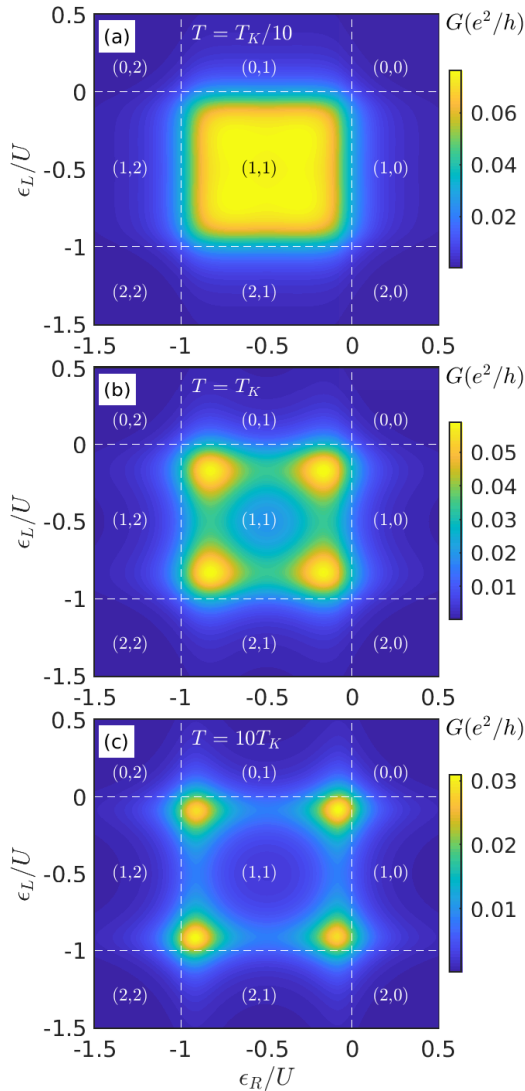


FIG. 2. The linear conductance  $G$  for nonmagnetic system calculated as a function of the position of each quantum dot level  $\varepsilon_L$  and  $\varepsilon_R$  for different temperatures: (a)  $T = T_K/10$ , (b)  $T = T_K$ , (c)  $T = 10T_K$ . The numbers in brackets indicate the occupation of each quantum dot,  $(\langle n_L \rangle, \langle n_R \rangle)$ , while the dashed lines separate the regions with different occupations. The parameters are:  $U = 0.2$ ,  $\Gamma = 0.015$  and  $t_{LR} = \Gamma/10$  in units of band halfwidth, and  $p = 0$ . The Kondo temperature is  $T_K \approx 0.0002$ .

such electric control, changing the magnetic configuration of the device will be another way to tune the spin-dependent behavior.

To begin with, in Fig. 2 we present the linear conductance  $G = \sum_{\sigma} G_{\sigma}$  as a function of quantum dot energy levels,  $\varepsilon_L$  and  $\varepsilon_R$ , in the case of nonmagnetic leads. We note that since the level positions can be changed by gate voltages, this figure effectively presents the gate voltage dependence of the conductance. The dashed lines in the figure mark the regions with different charges in the double dot, as indicated. This figure was determined for

three different temperatures,  $T = T_K/10$ ,  $T = T_K$  and  $T = 10T_K$ , where  $T_K$  is the Kondo temperature of a single dot in the case of  $\varepsilon_{\alpha} = -U/2$  and  $p = 0$ , which is approximately equal to [43]  $T_K \approx 0.0002$  in units of band halfwidth  $D$ , henceforth used as the energy unit  $D \equiv 1$ .

It is easy to understand the low values of conductance in the transport regions with even occupation on each quantum dot. Then, the Kondo effect between the dot and the corresponding lead does not develop and the spectral functions have relatively low weights, which effectively results in a suppressed conductance. When one of the dots is oddly occupied, it hosts the Kondo effect characterized by a pronounced resonance in the spectral function at the Fermi level. For single quantum dots coupled to the leads this would give rise to the unitary conductance through the system [12]. However, in the considered setup this is clearly not the case, as the Kondo effect on one of the dots does not result in large conductance through the whole system due to much lower spectral weight in the other dot. Only when the two quantum dots exhibit the Kondo effect at the same time, i.e. in the charge sector  $(1, 1)$ , the conductance through the system may become considerable. This is clearly visible in Fig. 2(a), which was calculated for  $T < T_K$ . For temperatures much lower than  $T_K$ , there is a plateau of relatively large  $G$  for  $-U \lesssim \varepsilon_L \lesssim 0$  and  $-U \lesssim \varepsilon_R \lesssim 0$ . This plateau is associated with the fact that both dots exhibit the Kondo effect in the single occupied regime. When the temperature is increased such that  $T = T_K$  (note that  $T_K$  is estimated for  $\varepsilon = -U/2$ ), one observes a gradual decrease of  $G$ , especially in the middle of the  $(1, 1)$  Coulomb blockade region, see Fig. 2(b). On the other hand, when  $T > T_K$ , the suppression becomes larger, such that only local maxima at the corners of the  $(1, 1)$  occupancy region are present, see Fig. 2(c). Assuming vanishing temperature and that each quantum dot exhibits the Kondo effect, the linear conductance is given by,

$$G \approx \frac{e^2}{h} \frac{8t_{LR}^2}{\Gamma^2}. \quad (9)$$

Note that the maximum value of the conductance is conditioned here by the value of the hopping between the dots, which is assumed to be much smaller than the coupling to external leads. This is why, although the conductance exhibits a plateau for  $T \ll T_K$ , its maximum value is still considerably lower than the unitary conductance.

Having presented the main features of the conductance in the nonmagnetic case, we are now ready to study the situation when the contacts are magnetic. We assume that the magnetizations of the leads can form two magnetic configurations, the parallel ( $P$ ) and antiparallel ( $AP$ ) one [5, 6]. Having determined the linear conductance in these two magnetic configurations,  $G_P$  and  $G_{AP}$ , we can calculate the tunneling magnetoresistance (TMR) of the device, which is defined as [9]

$$\text{TMR} = \frac{G_P - G_{AP}}{G_{AP}}. \quad (10)$$

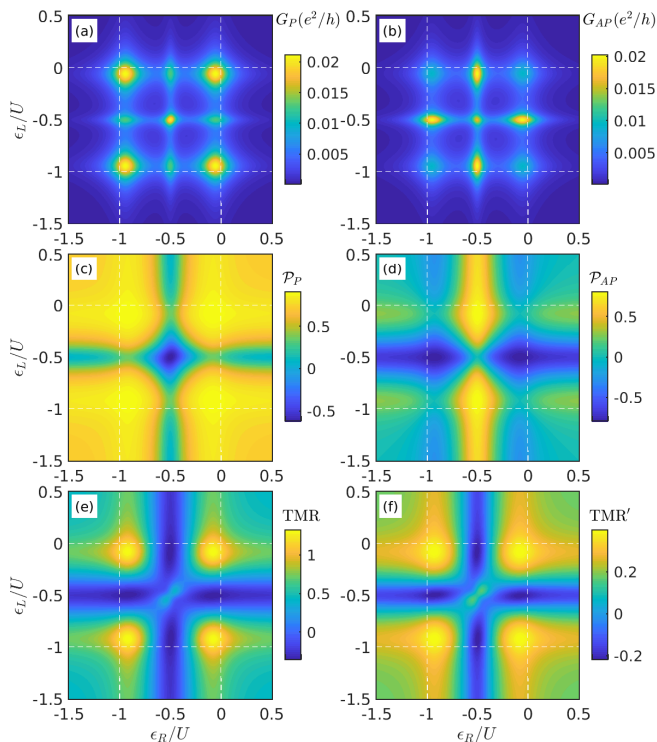


FIG. 3. (a,b) The linear conductance  $G_X$  and (c,d) current spin polarization  $\mathcal{P}_X$  in the case of (a,c) parallel ( $X = P$ ) and (b,d) antiparallel ( $X = AP$ ) magnetic configuration as well as the resulting tunnel magnetoresistance (e) TMR and (f) TMR' as a function of  $\varepsilon_L$  and  $\varepsilon_R$  for  $T = T_K$ . The dashed lines separate the regions with different occupations, as marked in Fig. 2. The parameters are the same as in Fig. 2 with  $p = 0.4$ .

We note that the TMR can be also defined in a different manner [35]

$$\text{TMR}' = \frac{G_P - G_{AP}}{G_P + G_{AP}}. \quad (11)$$

Because the two definitions result in different values of tunnel magnetoresistance and it is not easy to infer the value of e.g. TMR' from the knowledge of TMR, in the following, to make the picture complete, we present the both cases. Another important quantity characterizing the spin-resolved transport properties of the device is the spin polarization of the current. In the linear response regime it can be defined as

$$\mathcal{P}_X = \frac{G_{\uparrow}^X - G_{\downarrow}^X}{G_{\uparrow}^X + G_{\downarrow}^X}, \quad (12)$$

where  $G_{\sigma}^X$  is the linear conductance in the spin channel  $\sigma$  in the case of parallel ( $X = P$ ) or antiparallel ( $X = AP$ ) magnetic configuration.

The linear response conductance and spin polarization of the current in both magnetic configurations, as well as the tunnel magnetoresistance calculated as a function

of  $\varepsilon_L$  and  $\varepsilon_R$  at temperature  $T = T_K$  are presented in Fig. 3. We note that in the case of magnetic contacts the spin-resolved transport properties only weakly change for  $T \lesssim T_K$ , therefore we do not show the data for lower temperatures here. In fact, when  $T \ll T_K$ , it is only the conductance exactly for  $\varepsilon_L = \varepsilon_R = -U/2$  that becomes enhanced, while the other properties are hardly affected. This is associated with the fact that for  $\varepsilon_L = \varepsilon_R = -U/2$  the exchange fields cancel and both quantum dot local densities of states exhibit the Kondo resonance, resulting in an enhancement of linear conductance with lowering the temperature. At zero temperature, the conductance in the parallel and antiparallel magnetic configuration for  $\varepsilon_L = \varepsilon_R = -U/2$  can be approximated by

$$G_P \approx \frac{e^2}{h} \frac{8t_{LR}^2}{\Gamma^2} \frac{1+p^2}{(1-p^2)^2}, \quad (13)$$

$$G_{AP} \approx \frac{e^2}{h} \frac{8t_{LR}^2}{\Gamma^2} \frac{1}{1-p^2}. \quad (14)$$

It is interesting to note that for  $T \ll T_K$  both conductances are larger by a spin-polarization-dependent factor, as compared to the case of nonmagnetic leads, cf. Eq. (9). This is however only the case exactly in the middle of the (1,1) occupancy regime, since detuning from this point results in an immediate and large suppression of  $G$  due to the spin splitting of the orbital levels by the exchange field, see Figs. 3(a) and (b). In fact, the exchange field in each quantum dot,  $\Delta\varepsilon_{\text{exch}}^{\alpha}$ , plays a role of a local magnetic field that acts only on appropriate dot. Moreover, the magnitude and sign of this field can be controlled by purely electrical means, i.e. by tuning the gate voltages. This is clearly an asset of the setup discussed here over the magnetic field controlled spin valve demonstrated in Ref. [35].

Using the above formulas for the conductance in the case of  $\varepsilon_L = \varepsilon_R = -U/2$ , one can find the tunnel magnetoresistance,  $\text{TMR} \approx 2p^2/(1-p^2)$  and  $\text{TMR}' \approx p^2$ . On the other hand, the spin polarization in both magnetic configurations is  $\mathcal{P}_P \approx -2p/(1+p^2)$  and  $\mathcal{P}_{AP} \approx 0$ . It is interesting to note that the value of TMR for  $\varepsilon_L = \varepsilon_R = -U/2$  is the same as that predicted by the Julliere model for a single magnetic tunnel junction [9]. However, when the system is detuned from this point, the spin-resolved behavior becomes greatly changed. One can then observe both enhanced and inverse TMR effect as well as full current spin-polarization, which demonstrates a clear advantage of the considered DQD setup over a simple tunnel junction, as we show in the sequel.

When the system is detuned from the particle-hole symmetry point of each dot  $\varepsilon_L = \varepsilon_R = -U/2$ , the exchange field starts playing an important role and determines the system's transport properties. First of all, one can see that the conductance becomes then generally suppressed and it only shows lines of enhanced conductance in the (1,1) region for either  $\varepsilon_L = -U/2$  or  $\varepsilon_R = -U/2$ , see Figs. 3(a) and (b). For these values of the level position, there is a Kondo resonance in the local density of

states of one of the dots. Consequently, the cross-like feature visible in the middle Coulomb blockade region has the Kondo origin. In addition, there are also local maxima at the corners of the (1, 1) occupancy region, similarly as in the nonmagnetic case, cf. Fig. 2(b). These are related with enhanced tunneling processes when the dots are on resonance either for  $\varepsilon_\alpha \approx 0$  or  $\varepsilon_\alpha \approx -U$ . The above described behavior is present in both magnetic configurations. However, importantly, the magnitude of those effects is completely different, resulting in either positive or negative tunnel magnetoresistance, see Figs. 3(e) and (f). As far as the Kondo cross-like pattern is concerned, one can see that the TMR is negative in this parameter space, signaling that  $G_{AP} > G_P$ . This can be understood by realizing that when one of the dots is at half-filling its local density of states at low temperatures is given by  $A_{0\alpha}^\sigma = 1/\pi\Gamma_\alpha^\sigma$ . Assume that  $\varepsilon_L = -U/2$ , then for the linear conductance at  $T = 0$  one gets

$$G_{P/AP} \approx \frac{e^2}{h} \frac{4\pi t_{LR}^2}{(1-p^2)\Gamma} \left[ A_R^\uparrow(0) + A_R^\downarrow(0) \mp p(A_R^\uparrow(0) - A_R^\downarrow(0)) \right]. \quad (15)$$

Note that  $A_\alpha^\sigma(0)$  is the spectral function of dot  $\alpha$  for spin  $\sigma$  taken at the Fermi energy, which depends on the position of the dot level. Since, generally,  $A_R^\uparrow(0) > A_R^\downarrow(0)$  due to the strong coupling to the spin-up channel (except for  $\varepsilon_L = \varepsilon_R = -U/2$ ), one indeed finds that  $G_{AP} > G_P$ , resulting in inverse TMR effect. On the other hand, large values of conductance at the corners of the (1, 1) blockade region in the parallel magnetic configuration as compared to the antiparallel one are associated with enhanced transport properties in the majority spin channel. More specifically, in the parallel alignment the conductance is determined by a product of the local densities of states for the spin-up component which give the dominant contribution. In the antiparallel alignment, in turn,  $G_{AP}$  is always proportional to a product of the spin majority and spin minority densities of states. As a consequence, transport is more effective in the parallel configuration,  $G_P > G_{AP}$ , giving rise to positive TMR, see Figs. 3(e) and (f).

Let us now analyze the behavior of the spin polarization of the current shown in Figs. 3(c) and (d) for the two magnetic configurations. We note that the behavior for  $\varepsilon_L = \varepsilon_R = -U/2$  has already been discussed previously. The first general observation is that the behavior of the spin polarization is completely different depending on whether one of the dots is tuned to its particle-hole symmetry point  $\varepsilon_\alpha = -U/2$  or not. In the case of parallel configuration, when  $\varepsilon_\alpha = -U/2$  holds for one of the dots, the spin polarization is generally suppressed. This can be understood by resorting to low-temperature estimations, which, when assuming  $\varepsilon_L = -U/2$ , yield

$$\mathcal{P}_P \approx \frac{(1-p)A_R^\uparrow(0) - (1+p)A_R^\downarrow(0)}{(1-p)A_R^\uparrow(0) + (1+p)A_R^\downarrow(0)}. \quad (16)$$

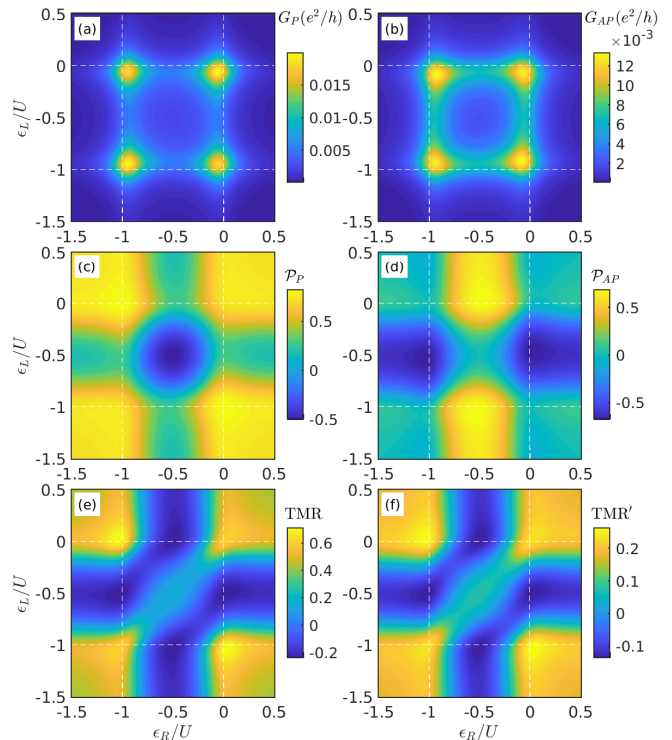


FIG. 4. The same as in Fig. 3 calculated for  $T = 10T_K$ .

It can be seen that the two terms in the numerator counterbalance each other resulting in suppressed  $\mathcal{P}_P$ . On the other hand, when  $\varepsilon_\alpha \neq -U/2$  for the two dots, the current is mainly determined by the majority spin channel, which results in large spin polarization of the current, reaching almost unity, see Fig. 3(c). A completely different situation can be observed for the antiparallel configuration, see Fig. 3(d). Now, when  $\varepsilon_\alpha \neq -U/2$ , one finds suppressed spin polarization, as the current is always proportional to a product of both majority and minority spin spectral functions. Nevertheless, when one of the dots exhibits the Kondo effect, i.e. when  $\varepsilon_\alpha = -U/2$  for one of the dots, large spin polarization can be found in the system. Moreover, the sign of  $\mathcal{P}_{AP}$  turns out to depend on whether  $\varepsilon_\alpha = -U/2$  for the left or for the right quantum dot. Again, this behavior can be understood assuming low-temperature limit. Consider first the case of  $\varepsilon_L = -U/2$ , one then finds

$$\mathcal{P}_{AP} \approx \frac{(1-p)A_R^\downarrow(0) - (1+p)A_R^\uparrow(0)}{(1+p)A_R^\uparrow(0) + (1-p)A_R^\downarrow(0)}. \quad (17)$$

At first sight, this formula may seem similar to Eq. (16). However, there are important differences, as now the spin-up (spin-down) component in the numerator is enhanced (suppressed) by a  $p$ -dependent factor. Taking additionally into account the fact that generally  $A_R^\uparrow(0) > A_R^\downarrow(0)$ , one can see that  $\mathcal{P}_{AP}$  becomes negative and reaches almost  $-1$ . The formula for  $\mathcal{P}_{AP}$  when  $\varepsilon_R = -U/2$  can be obtained from Eq. (17) by replac-

ing  $R \leftrightarrow L$  and changing the sign. Consequently, one then obtains  $\mathcal{P}_{AP} \rightarrow 1$ . This behavior is clearly seen in Fig. 3(d).

Figure 4 presents the same quantities as in Fig. 3 calculated for higher temperature,  $T = 10T_K$ . Since at this temperature the Kondo effect is smeared out by thermal fluctuations, no cross-like feature is visible in the conductance in the (1, 1) charge state regime, irrespective of the system's magnetic configuration, see Figs. 4(a) and (b). Instead, only the resonances at the corners of this blockade regime are present. As can be seen, basically all the features discussed in the case of  $T = T_K$  and visible in the behavior of spin polarization and tunnel magnetoresistance are also present for  $T = 10T_K$ . The main difference is that the most characteristic transport regimes are now broadened. In particular, in the case of parallel configuration, one finds enhanced  $\mathcal{P}_P$  only when each dot is evenly occupied, see Fig. 3(c). When one of the dots is singly occupied while the second dot's occupation is even,  $\mathcal{P}_P$  is reduced, whereas in the (1, 1) blockade regime the spin polarization becomes negative. An exactly opposite behavior can be seen for  $\mathcal{P}_{AP}$  [Fig. 3(d)]. Now, the spin polarization is suppressed whenever the total occupancy of the double dot is even, whereas for odd total occupation, one finds either  $\mathcal{P}_{AP} \rightarrow 1$  or  $\mathcal{P}_{AP} \rightarrow -1$ , depending on which dot is singly occupied, as already discussed previously. On the other hand, in the case of TMR one can observe that for higher temperatures the two definitions give qualitatively similar results, cf. Figs. 4(e) and (f), but of course there are still large quantitative differences. Positive magnetoresistance develops only when each of the dots has even occupancy, whereas in the other transport regimes, the TMR becomes negative except for a region along  $\varepsilon_L = \varepsilon_R$  in the (1, 1) occupation regime.

#### IV. NON-LINEAR RESPONSE REGIME

We now turn to the discussion of nonequilibrium transport properties and demonstrate that, in addition to the gate control discussed in previous section, the operation of the considered double quantum dot spin valve can be also tuned by applying the bias voltage. The current flowing through the system at finite bias voltage can be found from Eq. (6), whereas the tunnel magnetoresistance and the current spin polarization can be evaluated from Eqs. (10)-(12) by replacing the linear conductance with the nonequilibrium current. In the non-linear response regime, for left-right symmetric systems, the current satisfies the following relation  $I(V, \delta_L, \delta_R) = -I(-V, -\delta_L, -\delta_R)$ , where  $\delta_\alpha = 2\varepsilon_\alpha + U$  denotes the detuning from the particle-hole symmetry point of a given quantum dot. On the other hand, for the other quantities one has,  $X(V, \delta_L, \delta_R) = X(-V, -\delta_L, -\delta_R)$ , where  $X = \{G, \mathcal{P}, \text{TMR}, \text{TMR}'\}$ .

The current, differential conductance, current spin polarization and tunnel magnetoresistance as a function of bias voltage and the position of quantum dot levels

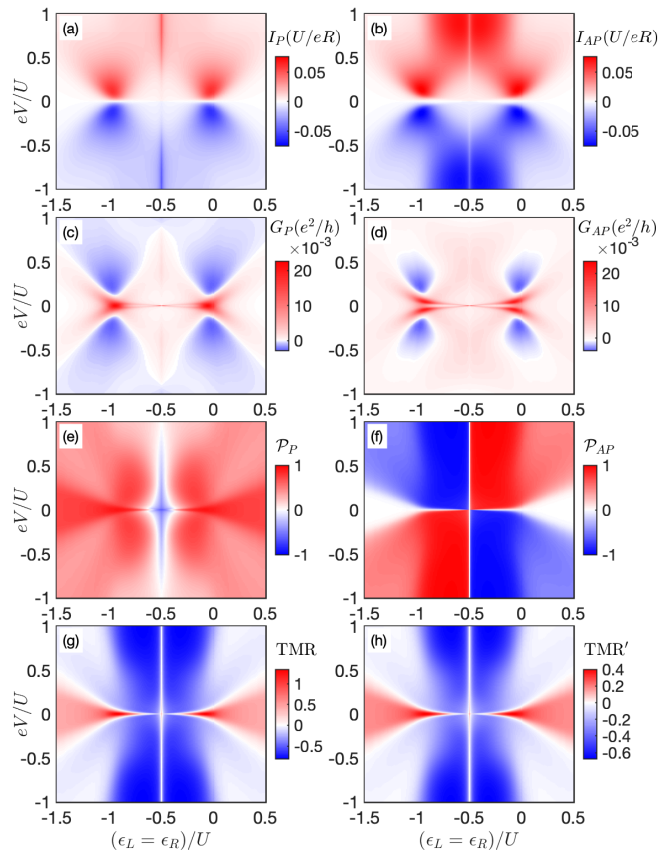


FIG. 5. (a,b) The current, (c,d) differential conductance, and (e,f) current spin polarization in the (left column) parallel and (right column) antiparallel configuration as well as (g,h) the tunnel magnetoresistance as a function of bias voltage  $V$  and position of the quantum dot levels  $\varepsilon_L = \varepsilon_R$ . The current is expressed in units of  $U/eR$ , where  $R = R_\uparrow + R_\downarrow$  is the resistance of the junction between the two dots in the case of nonmagnetic leads. The arrows indicate the value of  $\varepsilon_L = \varepsilon_R$  for which the spectral functions in Figs. 1(b) and (c) are presented. The parameters are the same as in Fig. 3 with  $T = 0$ .

$\varepsilon_L = \varepsilon_R$  are shown in Fig. 5. The current is plotted in units of  $U/eR$ , where  $R = R_\uparrow + R_\downarrow$  is the resistance of the tunnel junction between the quantum dots in the case of nonmagnetic leads. The relevant cross-sections of the density maps are shown in Fig. 6 for two selected values of the quantum dot level positions:  $\varepsilon_L = \varepsilon_R = -0.5U$  (left column) and  $\varepsilon_L = \varepsilon_R = -0.3U$  (right column), where the latter value corresponds to the case shown schematically in Figs. 1(b) and (c).

When the dot levels are kept equal, i.e.  $\varepsilon_L = \varepsilon_R$ , the exchange fields on each dot have the same magnitude and sign. Then, the change of system transport properties can be obtained by flipping the magnetization of one of the contacts and changing the magnetic configuration from parallel to antiparallel one. Such a situation is presented schematically in Figs. 1 (b) and (c), where the spectral functions for  $\varepsilon_L = \varepsilon_R = -0.3U$  are sketched.

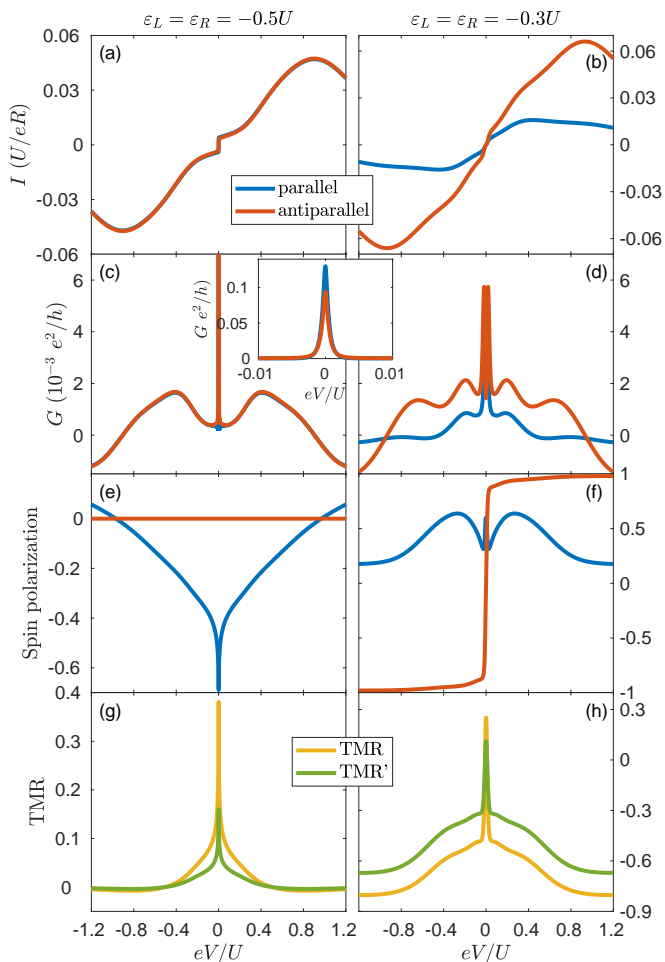


FIG. 6. (a,b) The current, (c,d) differential conductance and (e,f) current spin polarization in the parallel (blue) and antiparallel (red) magnetic configuration as well as (g,h) the tunnel magnetoresistance as a function of the bias voltage  $V$  calculated for (left column)  $\varepsilon_L = \varepsilon_R = -0.5U$  and (right column)  $\varepsilon_L = \varepsilon_R = -0.3U$ . The inset in (c) present a closeup of the differential conductance around the zero bias. The other parameters are the same as in Fig. 5.

For  $\varepsilon_L = \varepsilon_R > -U/2$ ,  $\Delta\varepsilon_{\text{exch}} < 0$ , such that each dot is occupied by a spin-up electron at equilibrium and the spectral function below the Fermi energy is mainly due to the spin-up component. In this case, when a finite bias is applied to the system, the current flowing through the device is very much suppressed at low temperatures. This is due to the mismatch in the densities of states: the occupied spin-up states from the left side do not have available states on the right side, since there the empty states are the spin-down ones, see Fig. 1 (b). To open the system and enable a considerable current to flow, one needs to change the magnetic configuration of the device. When the magnetization of the right electrode is flipped, the available states on the right are the spin-up states, see Fig. 1 (c), and a relatively large current can flow through the system. The difference in the currents in both magnetic configurations is nicely visible in Figs. 5(a) and (b).

Generally,  $|I_P| < |I_{AP}|$  except for the transport regime where both dots are evenly occupied (then the role of exchange field is diminished) and the voltage is sufficiently low. The difference in currents results in an inverse tunnel magnetoresistance, which develops in the regime of  $-U < \varepsilon_\alpha < 0$ , whereas for  $\varepsilon_\alpha > 0$  or  $\varepsilon_\alpha < -U$ , the magnetoresistance becomes positive, see Figs. 5(g) and (h).

Because the density of states of either side of the system is strongly energy- and spin-dependent, we observe that the current displays a nonmonotonic behavior, which is revealed in the negative differential conductance visible in Figs. 5(c) and (d) for the parallel and antiparallel magnetic configuration, respectively. At low bias voltages, one can observe signatures of the Kondo resonance, which is split due to the presence of exchange field, see the red sharp feature at low bias in Fig. 5(d). Such split Kondo resonance has already been observed experimentally for single quantum dots [5, 32, 33]. Note that the differential conductance exhibits a maximum at zero bias for  $\varepsilon_L = \varepsilon_R = -U/2$  due to the Kondo effect, where its low-temperature value is given by Eqs. (13) and (14). To demonstrate the behavior of conductance out of this special point, these maxima are not shown in Fig. 5, since they are much larger than the presented scale. These Kondo resonances are however nicely visible in the cross-sections shown in Fig. 6(c) and the corresponding inset.

Let us now have a look at the specific cross-sections of Fig. 5 and let us start with the case of  $\varepsilon_L = \varepsilon_R = -0.5U$  presented in the left column of Fig. 6. First we note that analytical formulas for the equilibrium values of the transport quantities have been presented in previous section. For  $\varepsilon_L = \varepsilon_R = -0.5U$ , the exchange field is not effective and the density of states is symmetric around the Fermi level with a pronounced Kondo resonance. Because of that, we observe moderate spin-resolved behavior: the currents are comparable for larger voltages, resulting in vanishing tunnel magnetoresistance, see Fig. 6(g). The main difference between the magnetic configurations is in fact visible at low bias, due to the different height of the Kondo resonance in both spin channels, which is then weakened as the voltage increases. As mentioned in previous section, the low bias behavior of the TMR for the DQD junction when  $\varepsilon_L = \varepsilon_R = -0.5U$  is similar to that of a single magnetic tunnel junction.

The situation however drastically changes when the dots' levels are detuned from the particle-hole symmetry point. The transport characteristics for this situation are presented in the right column of Fig. 6. Note that these results correspond exactly to the situations sketched in Figs. 1(b) and (c). Now, due to the reasons discussed above, the current in the antiparallel configuration is much larger than that in the parallel configuration, see Fig. 6(b). Moreover, as can be seen in Fig. 6(d), the Kondo resonance is now suppressed and split. The difference in currents is revealed in the magnetoresistance, which quickly drops and changes sign as the voltage is increased. In fact, for larger voltages,  $|eV| \gtrsim U/2$ , a



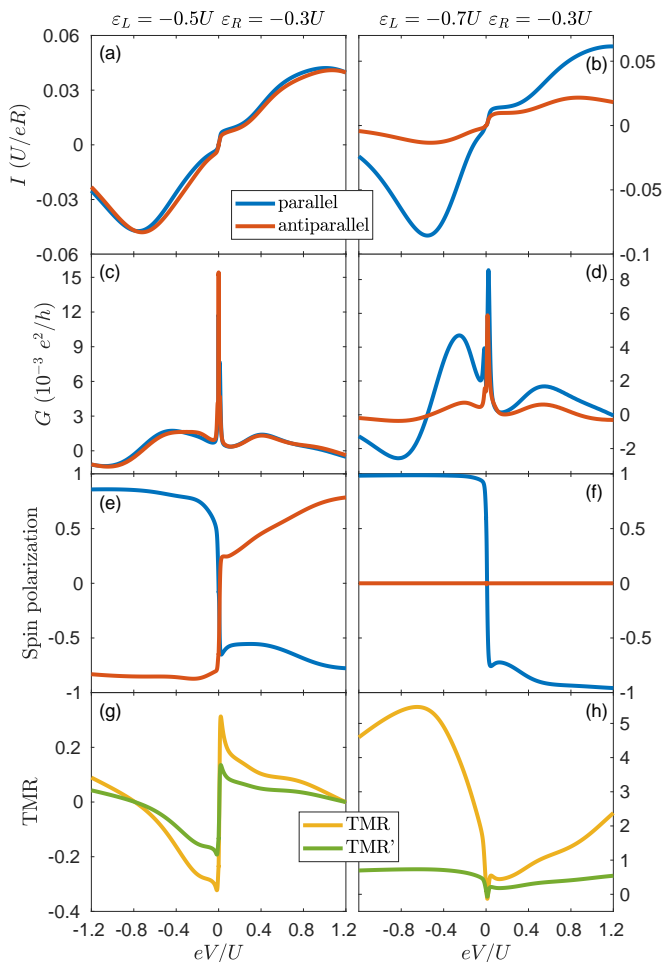


FIG. 7. (a,b) The current, (c,d) differential conductance and (e,f) current spin polarization in the parallel (blue) and antiparallel (red) magnetic configuration as well as (g,h) the tunnel magnetoresistance as a function of the bias voltage  $V$  calculated for  $\varepsilon_R = -0.3U$  and (left column)  $\varepsilon_L = -0.5U$  and (right column)  $\varepsilon_L = -0.7U$ . The other parameters are the same as in Fig. 5.

pronounced negative TMR develops in the system, revealing a considerable spin-valve behavior. Interestingly, one now also observes a very high spin polarization of the flowing current in the antiparallel configuration, reaching almost unity. The mechanism responsible for this large spin polarization is associated with high spin asymmetry in the density of states, as discussed above and shown schematically in Fig. 1.

Another way of controlling the spin-resolved properties of the considered spin valve is to tune the gate voltages and thus to adjust separately for each dot the local magnetic fields of exchange-field origin. This case is presented in Fig. 7, where we focus on the situation when the sign of the exchange field on the right dot is fixed, i.e.  $\Delta\varepsilon_{\text{exch}}^R < 0$ , favoring the spin-up (spin-down) electrons in the parallel (antiparallel) configuration. Note that the other situations can be obtained by

invoking the symmetry of the current with respect to the particle-hole symmetry point and the bias reversal,  $I(V, \delta_L, \delta_R) = -I(-V, -\delta_L, -\delta_R)$ . The left column of the figure presents the case when the exchange field is present only in one of the dots, while the other dot is tuned to the symmetry point. Even in this case the exchange field in one dot gives rise to enhanced spin polarization, which changes sign with either the bias reversal or the flip of magnetic configuration, see Fig. 7(e). However, the spin-valve behavior is rather moderate, with low values of tunnel magnetoresistance, see Fig. 7(g). To increase the difference in the current when the magnetic configuration of the system is varied, one needs to induce the spin splitting in both quantum dots—this case is presented in the right column of Fig. 7, which corresponds to the situation when the exchange fields have different signs, but the same magnitude. Due to the symmetry of densities of states, the current in the antiparallel configuration is now not spin polarized. However, a perfect current spin polarization is obtained in the case of parallel configuration, which is visible especially for negative bias voltage, see Fig. 7(f). This is just contrary to the case presented in Fig. 6(f), where large spin polarization was found in the antiparallel configuration. This demonstrates extremely high tunability of the device, obtained either by changing the alignment of magnetic moments of the leads or by tuning the level positions of the dots. It is now also clearly evident that if the exchange fields on both dots have different sign, an enhanced magnetoresistance can be generated in the system, see Fig. 7(h). Moreover, since the case presented in the left (right) column of Fig. 7 corresponds to the situation when the exchange field is present only in one of the dots (in both dots), comparing the two cases reveals advantages of the double quantum dot junction over a junction containing a single quantum dot.

Finally, we analyze the effect of different values of spin polarization as well as the impact of changing the coupling strength  $\Gamma$  on the spin-valve behavior of the system. The former case is presented in the left column of Fig. 8, while the latter case is displayed in the right column of this figure. We now only focus on the spin-resolved transport properties, i.e. on the current spin polarization and the tunnel magnetoresistance. Moreover, since  $\mathcal{P}_{AP}$  vanishes for the chosen set of level positions, we only present the behavior of  $\mathcal{P}_P$ . One can see that the current spin polarization is very high also for smaller values of  $p$  (especially for negative bias), and it approaches exactly unity with increasing  $p$ , see Fig. 8(a). The change of degree of the contacts' spin polarization has larger effect on the tunnel magnetoresistance. One can see that the higher  $p$ , the larger TMR the system exhibits. This is related with the fact that increasing  $p$  results in an enhancement of exchange field and, consequently, the magnetoresistive properties are also enlarged, see Figs. 8(c) and (e). On the other hand, if the coupling strength is changed while the spin polarization  $p$  is constant, one observes a strong impact on the behavior of the TMR, while  $\mathcal{P}_P$  rather

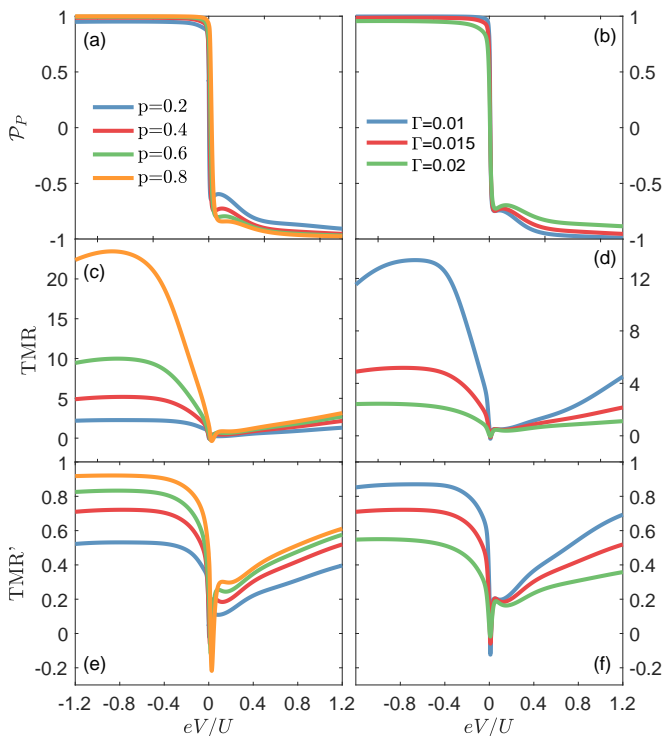


FIG. 8. (a,b) The current spin polarization in the parallel magnetic configuration and the tunnel magnetoresistance (c,d) TMR and (e,f) TMR' as a function of the bias voltage  $V$  calculated for  $\varepsilon_L = -0.7U$  and  $\varepsilon_R = -0.3U$  for different values of (left column) spin polarization and  $\Gamma = 0.015$  and (right column) for different values of coupling strength  $\Gamma$  and  $p = 0.4$ . The other parameters are the same as in Fig. 5.

weakly depends on the considered values of  $\Gamma$  (note that for negative bias the spin polarization is already essentially full anyway), see Fig. 8(a) and (b). In particular, the tunnel magnetoresistance for negative bias increases when  $\Gamma$  is lowered. This can be understood by realizing that for smaller couplings the width of resonant peaks in the local density of states decreases and their influence becomes suppressed. As a result, the difference between the opposite spin components of the spectral function in the singly occupied regime becomes enhanced, yielding increased magnetoresistance, see Figs. 8(d) and (f).

## V. CONCLUSIONS

We have analyzed the transport properties of a double quantum dot based spin valve, with each dot strongly coupled to its own ferromagnetic lead and weakly attached to each other. The current flowing through the system has been calculated perturbatively in the hopping between the dots, while the properties of a quantum

dot-ferromagnetic lead subsystem have been determined by using the numerical renormalization group method. This allowed us to capture all the electron correlations in an essentially exact manner. At low temperatures, the local density of states of the quantum dot-lead subsystem exhibits the Kondo resonance, which however becomes suppressed by the exchange field that splits the dot level when it is detuned from the particle-hole symmetry point. Consequently, by tuning the position of the quantum dot levels, one can adjust both the magnitude and sign of the spin splitting of the energy levels of the double dot. This enables a large voltage tunability of the device.

In the linear response regime, we have demonstrated that the tunnel magnetoresistance, associated with the change of magnetic configuration from the parallel to the antiparallel one, can reach large positive or negative values depending on the positions of the quantum dot levels. Moreover, we have also identified transport regimes of enhanced spin polarization of the linear conductance, which can be tuned by either changing the position of double dot levels or by switching the magnetic configuration of the device.

Finite bias voltage applied to the system provides another means of controlling the behavior of the considered spin valve. We have shown that one can obtain a perfect spin polarization of nonequilibrium current, whose sign can be controlled either by the gate voltages or by external magnetic field used to flip the magnetic configuration of the system. We have also predicted large magnetoresistance of the system in appropriate transport regime.

This work demonstrates that double quantum dots strongly attached to external ferromagnetic contacts behave as voltage-tunable spin valves with very prospective spin-resolved properties. The usage of an exchange field, which mimics magnetic field acting locally on a given quantum dot, is crucial for obtaining enhanced magnetoresistance and current spin polarization. It is beneficial over the usage of external magnetic field explored recently [35], and allows to obtain much larger magnetoresistive response of the system.

## ACKNOWLEDGMENTS

This work was supported by the Polish National Science Centre from funds awarded through the decision No. 2017/27/B/ST3/00621. S.C. acknowledges funding from SuperTop QuantERA network, the Ministry of Innovation and Technology and the NKFIH within the Quantum Information National Laboratory of Hungary, and the Quantum Technology National Excellence Program (Project Nr. 2017-1.2.1-NKP-122017-00001).

[1] Igor Žutić, Jaroslav Fabian, and S. Das Sarma, “Spintronics: Fundamentals and applications,” *Rev. Mod. Phys.* **76**, 323–410 (2004).

- [2] David D. Awschalom, Lee C. Bassett, Andrew S. Dzurak, Evelyn L. Hu, and Jason R. Petta, “Quantum Spintronics: Engineering and Manipulating Atom-Like Spins in Semiconductors,” *Science* **339**, 1174–1179 (2013).
- [3] J. Barnaś and A. Fert, “Magnetoresistance Oscillations due to Charging Effects in Double Ferromagnetic Tunnel Junctions,” *Phys. Rev. Lett.* **80**, 1058–1061 (1998).
- [4] W. Rudziński and J. Barnaś, “Tunnel magnetoresistance in ferromagnetic junctions: Tunneling through a single discrete level,” *Phys. Rev. B* **64**, 085318 (2001).
- [5] Abhay N. Pasupathy, Radosław C. Białczak, Jan Martinek, Jacob E. Grose, Luke A. K. Donev, Paul L. McEuen, and Daniel C. Ralph, “The Kondo Effect in the Presence of Ferromagnetism,” *Science* **306**, 86–89 (2004).
- [6] Sangeeta Sahoo, Takis Kontos, Jürg Furer, Christian Hoffmann, Matthias Gräber, Audrey Cottet, and Christian Schönberger, “Electric field control of spin transport,” *Nat. Phys.* **1**, 99–102 (2005).
- [7] J. Samm, J. Gramich, A. Baumgartner, M. Weiss, and C. Schönberger, “Optimized fabrication and characterization of carbon nanotube spin valves,” *J. Appl. Phys.* **115**, 174309 (2014).
- [8] J. Barnaś and I. Weymann, “Spin effects in single-electron tunnelling,” *J. Phys.: Condens. Matter* **20**, 423202 (2008).
- [9] M. Julliere, “Tunneling between ferromagnetic films,” *Phys. Lett. A* **54**, 225–226 (1975).
- [10] Sadamichi Maekawa, *Concepts in Spin Electronics (Series on Semiconductor Science and Technology (13))* (Oxford University Press, Oxford, England, UK, 2006).
- [11] Jun Kondo, “Resistance minimum in dilute magnetic alloys,” *Progress of Theoretical Physics* **32**, 37–49 (1964).
- [12] A. C. Hewson, *The Kondo problem to heavy fermions* (Cambridge University Press, 1997).
- [13] D. Goldhaber-Gordon, Hadas Shtrikman, D. Mahalu, David Abusch-Magder, U. Meirav, and M. A. Kastner, “Kondo effect in a single-electron transistor,” *Nature* **391**, 156 EP – (1998).
- [14] K. Hamaya, M. Kitabatake, K. Shibata, M. Jung, M. Kawamura, S. Ishida, T. Taniyama, K. Hirakawa, Y. Arakawa, and T. Machida, “Oscillatory changes in the tunneling magnetoresistance effect in semiconductor quantum-dot spin valves,” *Phys. Rev. B* **77**, 081302(R) (2008).
- [15] Ireneusz Weymann, “Finite-temperature spintronic transport through Kondo quantum dots: Numerical renormalization group study,” *Phys. Rev. B* **83**, 113306 (2011).
- [16] K. Hamaya, S. Masubuchi, M. Kawamura, T. Machida, M. Jung, K. Shibata, K. Hirakawa, T. Taniyama, S. Ishida, and Y. Arakawa, “Spin transport through a single self-assembled InAs quantum dot with ferromagnetic leads,” *Appl. Phys. Lett.* **90**, 053108 (2007).
- [17] Christopher A. Merchant and Nina Marković, “Electrically Tunable Spin Polarization in a Carbon Nanotube Spin Diode,” *Phys. Rev. Lett.* **100**, 156601 (2008).
- [18] Szabolcs Csonka, Ireneusz Weymann, and Gergely Zarand, “An electrically controlled quantum dot based spin current injector,” *Nanoscale* **4**, 3635–3639 (2012).
- [19] J. Martinek, Y. Utsumi, H. Imamura, J. Barnaś, S. Maekawa, J. König, and G. Schön, “Kondo effect in quantum dots coupled to ferromagnetic leads,” *Phys. Rev. Lett.* **91**, 127203 (2003).
- [20] Rosa López and David Sánchez, “Nonequilibrium Spintronic Transport through an Artificial Kondo Impurity: Conductance, Magnetoresistance, and Shot Noise,” *Phys. Rev. Lett.* **90**, 116602 (2003).
- [21] J. Martinek, M. Sindel, L. Borda, J. Barnaś, R. Bulla, J. König, G. Schön, S. Maekawa, and J. von Delft, “Gate-controlled spin splitting in quantum dots with ferromagnetic leads in the kondo regime,” *Phys. Rev. B* **72**, 121302 (2005).
- [22] Jürgen König and Jan Martinek, “Interaction-Driven Spin Precession in Quantum-Dot Spin Valves,” *Phys. Rev. Lett.* **90**, 166602 (2003).
- [23] Matthias Braun, Jürgen König, and Jan Martinek, “Theory of transport through quantum-dot spin valves in the weak-coupling regime,” *Phys. Rev. B* **70**, 195345 (2004).
- [24] Ireneusz Weymann, Jürgen König, Jan Martinek, Józef Barnaś, and Gerd Schön, “Tunnel magnetoresistance of quantum dots coupled to ferromagnetic leads in the sequential and cotunneling regimes,” *Phys. Rev. B* **72**, 115334 (2005).
- [25] N. M. Gergs, S. A. Bender, R. A. Duine, and D. Schuricht, “Spin Switching via Quantum Dot Spin Valves,” *Phys. Rev. Lett.* **120**, 017701 (2018).
- [26] Ireneusz Weymann, “Effects of different geometries on the conductance, shot noise, and tunnel magnetoresistance of double quantum dots,” *Phys. Rev. B* **78**, 045310 (2008).
- [27] Rok Žitko, Jong Soo Lim, Rosa López, Jan Martinek, and Pascal Simon, “Tunable Kondo Effect in a Double Quantum Dot Coupled to Ferromagnetic Contacts,” *Phys. Rev. Lett.* **108**, 166605 (2012).
- [28] Krzysztof P. Wójcik and Ireneusz Weymann, “Two-stage Kondo effect in T-shaped double quantum dots with ferromagnetic leads,” *Phys. Rev. B* **91**, 134422 (2015).
- [29] Ireneusz Weymann, Razvan Chirla, Piotr Trocha, and Cătălin Pașcu Moca, “SU(4) Kondo effect in double quantum dots with ferromagnetic leads,” *Phys. Rev. B* **97**, 085404 (2018).
- [30] K. Hamaya, M. Kitabatake, K. Shibata, M. Jung, M. Kawamura, K. Hirakawa, T. Machida, T. Taniyama, S. Ishida, and Y. Arakawa, “Electric-field control of tunneling magnetoresistance effect in a  $x\text{N-NiInAsNi-zf7de}$  quantum-dot spin valve,” *Appl. Phys. Lett.* **91**, 022107 (2007).
- [31] K. Hamaya, M. Kitabatake, K. Shibata, M. Jung, M. Kawamura, K. Hirakawa, T. Machida, T. Taniyama, S. Ishida, and Y. Arakawa, “Kondo effect in a semiconductor quantum dot coupled to ferromagnetic electrodes,” *Appl. Phys. Lett.* **91**, 232105 (2007).
- [32] J. R. Hauptmann, J. Paaske, and P. E. Lindelof, “Electric-field-controlled spin reversal in a quantum dot with ferromagnetic contacts,” *Nat. Phys.* **4**, 373 (2008).
- [33] M. Gaass, A. K. Hüttel, K. Kang, I. Weymann, J. von Delft, and Ch. Strunk, “Universality of the Kondo Effect in Quantum Dots with Ferromagnetic Leads,” *Phys. Rev. Lett.* **107**, 176808 (2011).
- [34] Alois Dirnaignner, Milena Grifoni, Andreas Prüfling, Daniel Steininger, Andreas K. Hüttel, and Christoph Strunk, “Transport across a carbon nanotube quantum dot contacted with ferromagnetic leads: Experiment and nonperturbative modeling,” *Phys. Rev. B* **91**, 195402 (2015).
- [35] Arunav Bordoloi, Valentina Zannier, Lucia Sorba, Christian Schönberger, and Andreas Baumgartner, “A double quantum dot spin valve,” *Commun. Phys.* **3**, 1–7

- (2020).
- [36] P. W. Anderson, “Localized magnetic states in metals,” *Phys. Rev.* **124**, 41 (1961).
- [37] Yuli V. Nazarov and Yaroslav M. Blanter, *Quantum Transport: Introduction to Nanoscience* (Cambridge University Press, Cambridge, England, UK, 2009).
- [38] Kenneth G. Wilson, “The renormalization group: Critical phenomena and the kondo problem,” *Rev. Mod. Phys.* **47**, 773–840 (1975).
- [39] We used the open-access Budapest Flexible DM-NRG code, <http://www.phy.bme.hu/~dmnrg/>; O. Legeza, C. P. Moca, A. I. Tóth, I. Weymann, G. Zaránd, arXiv:0809.3143 (2008) (unpublished).
- [40] Ralf Bulla, Theo A. Costi, and Thomas Pruschke, “Numerical renormalization group method for quantum impurity systems,” *Rev. Mod. Phys.* **80**, 395–450 (2008).
- [41] M. Yoshida, M. A. Whitaker, and L. N. Oliveira, “Renormalization-group calculation of excitation properties for impurity models,” *Phys. Rev. B* **41**, 9403–9414 (1990).
- [42] Axel Freyn and Serge Florens, “Optimal broadening of finite energy spectra in the numerical renormalization group: Application to dissipative dynamics in two-level systems,” *Phys. Rev. B* **79**, 121102 (2009).
- [43] F. D. M. Haldane, “Scaling theory of the asymmetric anderson model,” *Phys. Rev. Lett.* **40**, 416–419 (1978).